Title	Strength-enhanced Sn-In low-temperature alloy with surface-modified ZrO₂ nanoparticle addition
Author(s)	Nitta, Shunya; Tatsumi, Hiroaki; Nishikawa, Hiroshi
Citation	Journal of Materials Science: Materials in Electronics. 2023, 34(31)
Version Type	VoR
URL	https://hdl.handle.net/11094/93291
rights	This article is licensed under a Creative Commons Attribution 4.0 International License.
Note	

Strength-enhanced Sn–In low-temperature alloy with surface-modified ZrO$_2$ nanoparticle addition

Shunya Nitta[1,*] , Hiroaki Tatsumi[2] , and Hiroshi Nishikawa[2,*]

[1] *Graduate School of Engineering, Osaka University, 2-1 Yamadaoka, Suita, Osaka 565-0871, Japan*
[2] *Joining and Welding Research Institute, Osaka University, 11-1 Mihogaoka, Ibaraki, Osaka 567-0047, Japan*

ABSTRACT

Low-temperature packaging is essential for the widespread use of flexible electronic devices, and Sn–In eutectic alloys have attracted considerable attention because of their low melting temperatures. However, these alloys have a lower strength compared with other types of solder alloys. This study aimed to investigate the effect of adding nanoparticles on the mechanical strength of Sn–In eutectic alloys while keeping their melting temperature unchanged. ZrO$_2$ nanoparticles coated with NiO (NiO/ZrO$_2$ nanoparticles) were utilized to strengthen Sn–In eutectic alloys with a high dispersity. Sn–In composite alloys reinforced with NiO/ZrO$_2$ nanoparticles were fabricated, and tensile strength evaluation and microstructure observations were conducted. The experimental results showed that the addition of nanoparticles to the Sn–In eutectic alloys did not change their melting behavior. The tensile strength of the Sn–In composite alloys reinforced with NiO/ZrO$_2$ nanoparticles increased by up to 35.6%, which was attributed to grain refinement and dispersion strengthening. Even after thermal aging at 60 ºC, the Sn–In composite alloys reinforced with NiO/ZrO$_2$ nanoparticles showed a 1.11 times higher ultimate tensile strength than that of the non-aged, non-reinforced eutectic alloy, despite grain coarsening. This was attributed to the contribution of dispersion strengthening. These results indicate that the addition of NiO/ZrO$_2$ nanoparticles is an effective method to improve the strength of low-melting-temperature alloys.

1 Introduction

Initiatives related to the Sustainable Development Goals have recently attracted increasing attention to environmental issues, including the control of hazardous waste. In electronics manufacturing, Pb-free solders are in high demand because of the toxicity of Pb. Moreover, current electronic devices require flexibility, which enables them to easily fit into complex shapes [1, 2]. Therefore, flexible substrates composed of thin heat-sensitive resin films have been widely developed [3]. Such flexible substrates show good versatility for a wide variety of flexible devices; however, their temperature tolerance remains a major issue, especially against high-temperature exposure during the soldering process. Zardetto et al. [4] reported

Address correspondence to E-mail: nitta.shunya.gvc@ecs.osaka-u.ac.jp; nishikawa@jwri.osaka-u.ac.jp

that the electrical resistance of a flexible substrate increased significantly at 180 °C or higher. The maximum temperature during the soldering process using Sn–Ag–Cu solder (SAC), which is the most widely used as Pb-free solder, was approximately 250 °C [5, 6]. Therefore, the development of low-melting-temperature solders is urgently required.

Sn–Bi and Sn–In alloys are promising low-melting temperature solders. The eutectic Sn–Bi and Sn–In alloys show significantly low melting temperatures of 139 and 119 °C [7]. Each of these alloys has its advantages and disadvantages. In general, the brittleness of Sn–Bi eutectic alloys is a critical problem affecting the reliability of solder joints [8, 9], which also show limited flexibility. In addition, the formation whiskers under high-temperature and stress-loaded conditions leads to poor electrical reliability in Sn–Bi solders [10]. In contrast, Sn–In alloys exhibit a lower melting temperature and superior elongation than Sn–Bi alloys. Notably, In is a ductile soft metal. These characteristics are advantageous for flexible-device applications. However, the low tensile strength of Sn–In alloys is a critical issue. Han et al. [11] reported that the ultimate tensile strength of the eutectic Sn–In alloy was approximately 11.0 MPa, which is lower than that of Sn–1.0Ag–0.5Cu alloy, 27.3 MPa [12], and of Sn–Bi eutectic alloy, 60 MPa [13]. Therefore, an improvement in the ultimate tensile strength is desired.

There are two main methods for solder reinforcement. One is the fabrication of new alloys by adding elements and the other is the fabrication of composite materials by adding nanoparticles. The creation of new alloys by adding elements is characterized by the fact that effects other than increased strength can be obtained. For example, the melting temperature can be controlled and elongation can be promoted. Han et al. reported that the addition of 0.5–1.5 mass% Ag to Sn–In eutectic solders can promote elongation [11]. Kanlayasiri et al. reported that the addition of 3 mass% In to Sn–0.3Ag–0.7Cu solder lowered the solidus and liquidus temperatures by 21.7 and 11.5 °C, respectively [14]. However, the Sn–In eutectic solder inherently exhibits sufficient elongation and has a low melting point; therefore, the fabrication of composite materials by adding nanoparticles was investigated in this study.

The use of various additives in solders has been widely investigated as a strengthening method. The addition of nanoparticles such as Al_2O_3, Mo, and ZrO_2 to improve joint strength has recently been investigated [15–17]. An advantage of nanoparticle-containing solders, commonly called composite solders, is that the added nanoparticles rarely react and do not form intermetallic compounds (IMCs) in the solder matrix. They enable solder microstructure refinement by acting as nucleation sites during solidification [18]. Adding nanoparticles also provides a strengthening effect based on the dispersion strengthening mechanism [19]. The refinement and dispersion strengthening effects of nanoparticle addition are beneficial in improving the strength of the Sn–In alloy.

Al_2O_3 and ZrO_2 are potential nanoparticle materials that can be added to solder alloys. Ceramic nanoparticles, which are nonreactive with the solder matrix, are typically used as additives. According to Shen et al. [18], the addition of ZrO_2 to the SAC solder suppresses the growth of chemical reaction layers without changing the melting temperature and improves the Vickers hardness of the solder. Amares et al. [20] reported that the addition of ZrO_2 to Sn–Bi eutectic alloys improved their tensile strength. However, the high surface energy of nanoparticles may cause aggregation in the alloy. Therefore, modifying the surface of nanoparticles is beneficial. Huo et al. [21] demonstrated that ZrO_2 nanoparticles covered by a NiO layer (NiO/ZrO_2 nanoparticles) were homogeneously distributed within a Sn–1.0Ag–0.5Cu solder matrix. Based on their findings, NiO/ZrO_2 nanoparticles are expected to be promising additives for Sn–In-based composite alloys.

Therefore, the purpose of this study is to investigate the ultimate tensile strength of Sn–In composite alloys reinforced with NiO/ZrO_2 nanoparticles and to clarify the effects of nanoparticle addition on microstructure and mechanical properties. Sn–In composite alloys reinforced with NiO/ZrO_2 nanoparticles at various content ratios were fabricated. First, the melting behavior was evaluated using thermal analysis. Next, tensile tests were performed on the composite alloys to investigate the effect of nanoparticle content ratio on the mechanical properties. The microstructure of the composite alloy was investigated using electron microscopy, focusing on the morphology and grain size of the constituent phases. In addition, to investigate the effect of thermal aging on the microstructure and mechanical properties of the composite alloys, an aging test was performed at 60 °C for 1008 h. Based on these results, the effects of adding NiO/ZrO_2 nanoparticles to the Sn–In eutectic alloy and the mechanism of strength enhancement were discussed.

2 Experimental procedure

2.1 Fabrication of Sn–In composite alloys reinforced with NiO/ZrO₂

Sn–52In (mass%) eutectic alloy (Senju Metal Industry Corporation, Japan) reinforced with NiO/ZrO$_2$ nanoparticles was evaluated. NiO/ZrO$_2$ nanoparticles were prepared by ball-milling pyrolysis using ZrO$_2$ nanoparticles (HW Nanomaterials, China) and Ni(CH$_3$COO)$_2$·4H$_2$O (Wako Pure Chemicals Corporation, USA) as raw materials. ZrO$_2$ nanoparticles with a purity of 99.9% and a particle size distribution of 60–120 nm were used. NiO with a size of approximately 8.8 nm was uniformly and densely attached to the surface of the ZrO$_2$ nanoparticles. The detailed procedure of the ball-milling pyrolysis method was described in our previous report [21].

Figure 1 shows a schematic of the fabrication process for the composite alloy. The commercial Sn–In alloy was heated to 300 °C in a furnace in air, as shown in Fig. 1(a). Subsequently, different mass fractions (0, 0.1, 0.2, 0.3, 0.4, and 0.5 mass%) of NiO/ZrO$_2$ nanoparticles were added to the molten alloy, as shown in Fig. 1(b). An ultrasonic homogenizer was then applied to the mixture consisting of the molten alloy and NiO/ZrO$_2$ nanoparticles, as shown in Fig. 1(c). The ultrasonic treatment time was 240 s. After removing the oxide film from the molten alloy surface, the molten alloy was cast into an iron mold with dimensions of 50 mm × 10 mm × 5 mm.

2.2 Characterization and testing

The melting behavior of the composite alloys reinforced with various NiO/ZrO$_2$ nanoparticle contents was examined using differential scanning calorimetry (DSC) (7020 clinical analyzers, Hitachi High Tech Science Corporation, Japan) under an N$_2$ constant flow of 50 mL/s. The subjected alloys were heated up to 250 °C at a heating rate of 10 °C /min. The onset and offset temperatures of each composite alloy were evaluated from the obtained curves.

The composite alloys were shaped into dumbbells by wire electrical discharge machining (Sodick AG 360 L, Kobayashi Kikai, Japan) for the tensile tests. The dimensions of the dumbbells are shown in Fig. 2. The thickness and width of the parallel section were 1 and 2 mm, respectively, and the corresponding gauge length was 10 mm. Tensile testing was conducted under an initial strain rate of $5·10^{-4}$ s^{-1} using a universal tensile machine (Autograph AG–X, Shimadzu, Japan). Eight tests were conducted on each composite alloy. The elongation and ultimate tensile strength were determined using tensile stress–strain curves. The fracture surfaces of the tensile specimens were examined by scanning electron microscopy (SEM) (JSM-IT200, JEOL, Japan).

The microstructures of the cross-sectioned composite alloys were observed by SEM after grinding with SiC grit paper in the order of #800, #1200, and #2000, followed by successive polishing with 1.0 and
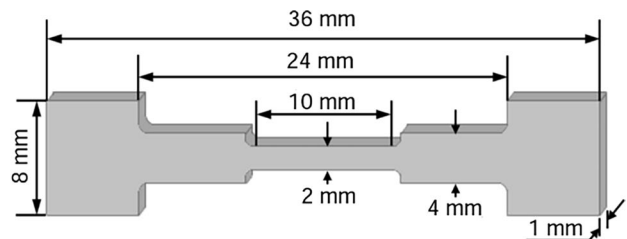
**Fig. 2** Schematic of the typical tensile test specimen
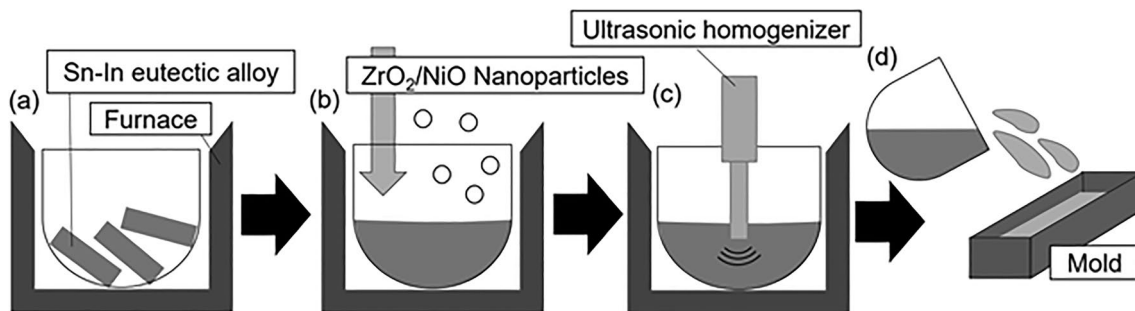
Fig. 1 Schematic of the experimental procedure of (a) melting process, (b) nanoparticle addition, (c) agitation process, and (d) casting process

0.3 μm alumina suspensions. The grain sizes of the composite alloys were calculated by drawing a test line and counting the number of times a grain crossed the line using the image-editing software Image J [22]. To investigate the effect of thermal aging on microstructure and mechanical properties of the composite alloys, they were placed in an oil bath at 60 °C for 168, 504, and 1008 h. Silicone oil was used to prevent oxidation of the samples during exposure to high temperatures. The sample surfaces were washed with ethanol after thermal aging. Tensile tests and microstructural observations were conducted.

3 Results

3.1 Melting behavior

Thermal analysis using DSC was performed to clarify the effect of nanoparticle addition on melting behavior. Figure 3 shows the DSC results. Table 1 summarizes the onset temperature (T_{on}) and offset temperature (T_{off}) obtained from the DSC results. The lowest onset temperature was 110.3 °C at 0.5 mass%, and the highest was 111.6 °C at 0.1 mass% addition. These results indicated that NiO/ZrO$_2$ nanoparticle addition has a negligible effect on melting behavior. Amares et al. performed differential scanning calorimetry on Sn–Bi eutectic alloys with ZrO$_2$ nanoparticles and found that
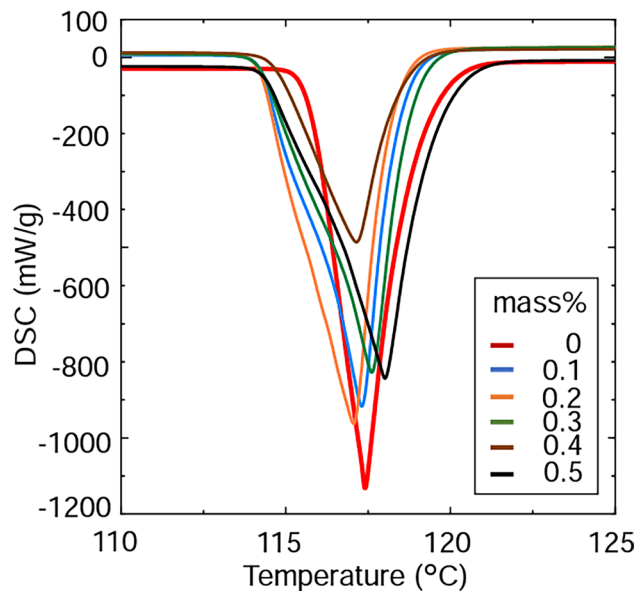
**Table 1** Melting properties of the Sn–In composite solders reinforced with 0–0.5 mass% of NiO/ZrO$_2$ nanoparticles

Addition amount (mass%)	T_{on} (°C)	T_{off} (°C)
0	110.9	123.3
0.1	111.6	121.6
0.2	111.4	121.4
0.3	110.9	121.7
0.4	111.3	121.6
0.5	110.3	123.7

the maximum difference in the solidus temperature was 0.9 °C in the case of 0.4 mass% [20]. Chang et al. performed DSC on aSn–3.5Ag–0.7Cu solder with TiO [23], obtaining an increase value of approximately 0.5 °C, which is a minor change. Therefore, previous studies also support the idea that the addition of ceramic nanoparticles to alloys does not change their melting behavior. This is a good indication for this study, which aimed to maintain a low melting temperature.

3.2 Mechanical properties

To clarify the effect of ZrO$_2$/NiO nanoparticles on the mechanical properties, tensile tests were conducted on composite alloys with various nanoparticle contents. Figure 4(a) shows typical stress–strain curves of the Sn–In composite alloys reinforced with NiO/ZrO$_2$ nanoparticles. At 0–0.1 mass%, the curves showed good elongation but a low ultimate tensile strength. On the other hand, at 0.2–0.5 mass%, the curves showed high tensile strength but low elongation. Figure 4(b) shows the average ultimate tensile strength values. The average ultimate tensile strength was 8.56 MPa at 0 mass% ZrO$_2$/NiO nanoparticles. Upon adding 0.1, 0.2, 0.3, 0.4, and 0.5 mass% ZrO$_2$/NiO nanoparticles, the average ultimate tensile strengths were 10.4 (+ 21.5%), 10.7 (+ 25.0%), 10.7 (+ 25.0%), 11.6 (+ 35.6%), and 10.5 MPa (+ 22.7%). Thus, the ultimate tensile strength increased with increasing ZrO$_2$/NiO nanoparticle content up to 0.4 mass%, reaching a maximum value of 11.62 MPa. The ultimate tensile strength at 0.5 mass% decreased slightly to 10.53 MPa. Figure 4(c) shows the average elongation values. The average elongation value was 49.9% at 0 mass% ZrO$_2$/NiO nanoparticles. Upon adding 0.1, 0.2, 0.3, 0.4, and 0.5 mass% ZrO$_2$/NiO nanoparticles, the average elongation values were 40.3 (− 19.4%), 26.5 (− 47.0%), 13.6 (− 72.8%), 13.4

Fig. 3 DSC curves of the Sn–In composite solders reinforced with 0–0.5 mass% of NiO/ZrO$_2$ nanoparticles

Fig. 4 Tensile test results of the Sn–In composite solders reinforced with 0–0.5 mass% of NiO/ZrO$_2$ nanoparticles: **a** stress–strain curves **b** tensile strength and **c** elongation
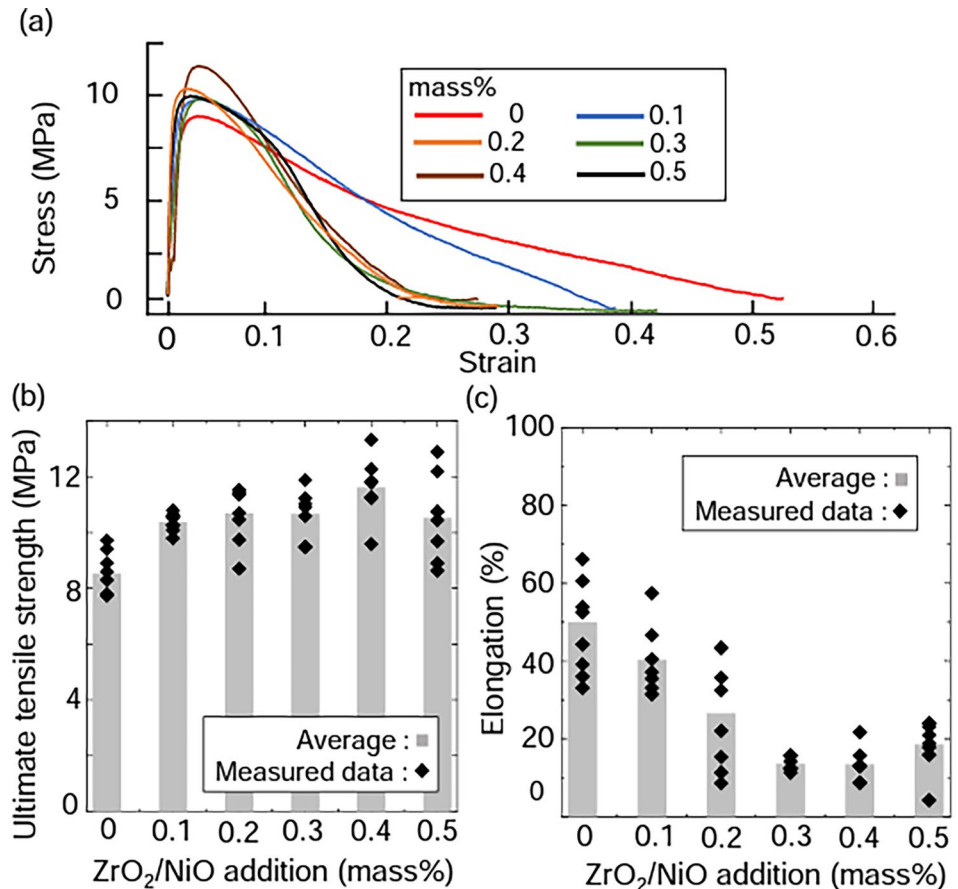

(− 73.2%), and 18.6% (− 62.8%), respectively. Thus, the elongation decreased with increasing ZrO$_2$/NiO nanoparticle content up to 0.4 mass%, reaching a minimum elongation value of 13.4%.

Fracture surface observations were conducted to investigate the effect of nanoparticle addition on the fracture behavior. Figure 5 shows the optical and SEM fracture surfaces of the composite alloys reinforced with the addition of 0, 0.3, and 0.5 mass% ZrO$_2$/NiO nanoparticles. As shown in Fig. 5, the composite alloys with 0, 0.3, and 0.5% ZrO$_2$/NiO exhibited different optical fracture morphologies, namely chisel point, shear, and brittle fracture morphologies, respectively. In general, the ductility improves as the fracture morphology changes from brittle to shear to chisel point [24, 25]. Therefore, the decrease in elasticity is expected with increasing nanoparticle additions. The SEM images showed that the fracture surface at 0 mass% had a characteristic flat area (circled), while at 0.3 mass%, the fracture surface was mostly uneven, with no flat areas. At 0.5 mass%, a mixture of flat and uneven areas was observed.

3.3 Microstructure

Microstructural observations were performed using SEM to investigate the effect of the nanoparticle addition on the microstructure. Figure 6 shows the microstructures of the Sn–In composite alloys reinforced with various ZrO$_2$/NiO nanoparticle contents. Two phases with convex and covering morphologies were observed in the Sn–In alloy without the addition of nanoparticles, as shown in Fig. 6 (a). Comparison of the alloy phase diagram with the results of the EDS analysis shows that the phases with convex and covering morphologies are γ-phase (Sn$_4$In) and β-phase (SnIn$_3$), respectively. This is consistent with the results of Ref. [26]. These two phases were also observed in the Sn–In composite alloys reinforced with ZrO$_2$/NiO nanoparticles, indicating that the addition of ZrO$_2$/NiO nanoparticles did not cause a phase change. However, the addition of ZrO$_2$/NiO nanoparticles resulted in changes in the microstructural morphology and grain size. The γ-Sn phase was
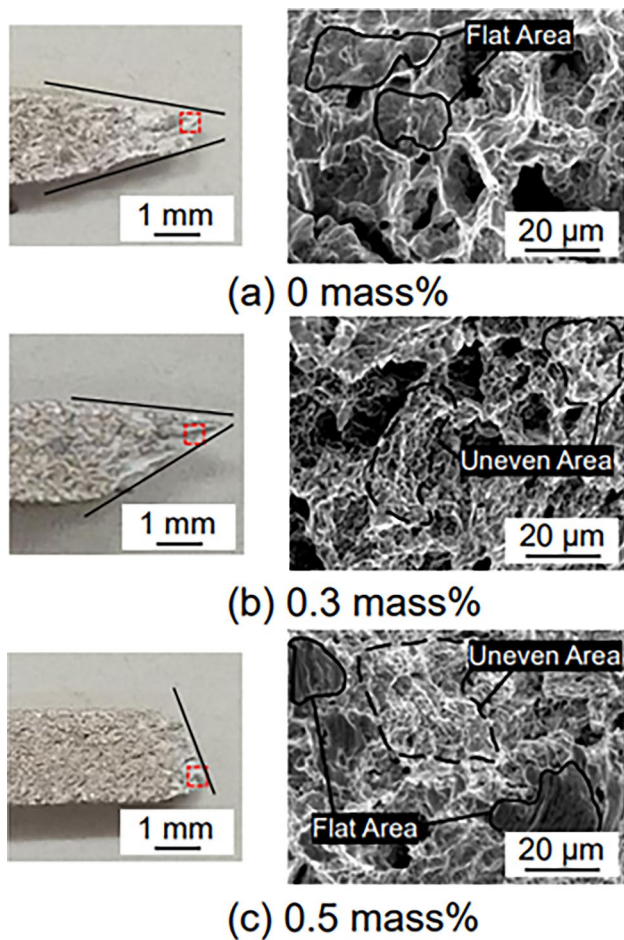
Fig. 5 Optical and SEM images of fracture surfaces of the Sn–In composite solders reinforced with **a** 0, **b** 0.3, and **c** 0.5 mass% of NiO/ZrO$_2$ nanoparticles

rounded when the addition of ZrO$_2$/NiO nanoparticles was 0 and 0.5 mass%. At 0.1–0.4 mass%, the γ-Sn phase was sharply elliptical, confirming the layered structure of the γ-Sn and β-In phases. Figure 7 shows the results of the average grain size measurements. The average grain size was 15.2 µm when the addition of ZrO$_2$/NiO nanoparticles was 0 mass%. Upon adding 0.1, 0.2, 0.3, 0.4, and 0.5 mass% ZrO$_2$/NiO nanoparticles, the grain sizes were 7.24 (− 52.4%), 7.11 (− 53.2%), 6.72 (− 55.8%), 4.72 (− 68.8%), and 15.7 µm (+ 3.29%), respectively. The grain sizes when the addition was 0 and 0.5 mass% were equivalent, at approximately 15 µm; those when the addition was 0.1–0.4 mass% were also equivalent, at approximately 7 µm. Microstructural observations indicated

that the addition of appropriate amounts of nanoparticles refined the microstructure.

3.4 Thermal aging

Thermal aging at 60 °C was performed to investigate the changes in ultimate tensile strength and elongation of Sn–In composite alloys reinforced with various ZrO$_2$/NiO nanoparticle contents. Figure 8 shows the relationship between the aging time and the average ultimate tensile strength and elongation of the reinforced alloys. Figure 8a shows that the ultimate tensile strength decreased slightly with increasing aging time for all the nanoparticle contents. At 0 mass%, the ultimate tensile strength slightly decreased from 8.56 MPa to 7.87 MPa after aging for 1008 h. At 0.4 mass%, the ultimate tensile strength slightly decreased from 11.6 MPa to 9.11 MPa after aging for 1008 h. Even after the aging, the ultimate tensile strength of the Sn–In composite alloy reinforced with 0.4 mass% addition was 15.8% higher than that of the alloy without nanoparticles.

Figure 8b shows the difference in the elongation change tendency with aging time depending on the nanoparticle amount. At 0, 0.1, and 0.2 mass%, the elongation significantly decreased with increasing aging time; e.g., the elongation at 0 mass% before and after aging for 1008 h was 49.9 and 30.4%, respectively. In contrast, at 0.3 and 0.4 mass%, the elongations were almost constant regardless of aging time; e.g., the elongations at 0.4 mass% before and after aging for 1008 h were 13.4 and 16.8%, respectively. The Sn–In composite alloys reinforced with 0.3–0.4% nanoparticles showed lower elongations than those of the other alloys in the initial state; however, they showed stable elongation characteristics against aging.

Fracture surface observations were performed to investigate the effect of aging at 60 °C on the fracture behavior of Sn–In composite alloys reinforced with various ZrO$_2$/NiO nanoparticle contents. Figure 9 shows the optical and SEM fracture surfaces of the composite alloys reinforced with 0 and 0.4 mass% ZrO$_2$/NiO, showing that the fracture surface at 0 mass% is a shear fracture surface with a 45° fracture plane, while at 0.4 mass%, it is a brittle fracture surface with a horizontal fracture plane. Compared with the state before thermal aging, as shown in Fig. 5, the 0.4 mass% addition resulted in negligible difference. However, without the nanoparticle addition, the reduced elongation can be ascribed to the large

Fig. 6 SEM microstructure images of the Sn–In composite solders reinforced with **a** 0, **b** 0.1, **c** 0.2, **d** 0.3, **e** 0.4, and **f** 0.5 mass% of NiO/ZrO$_2$ nanoparticles
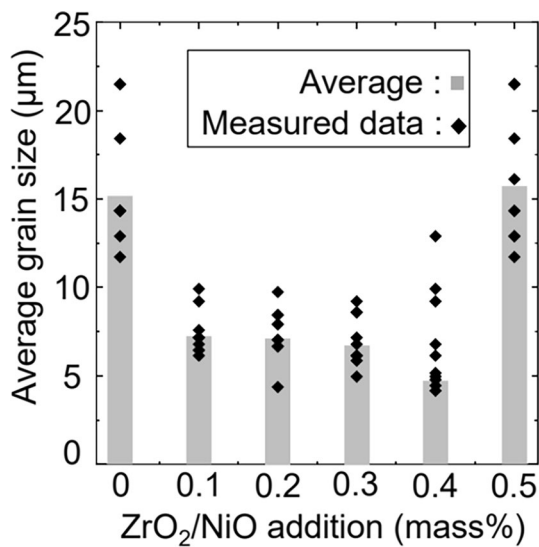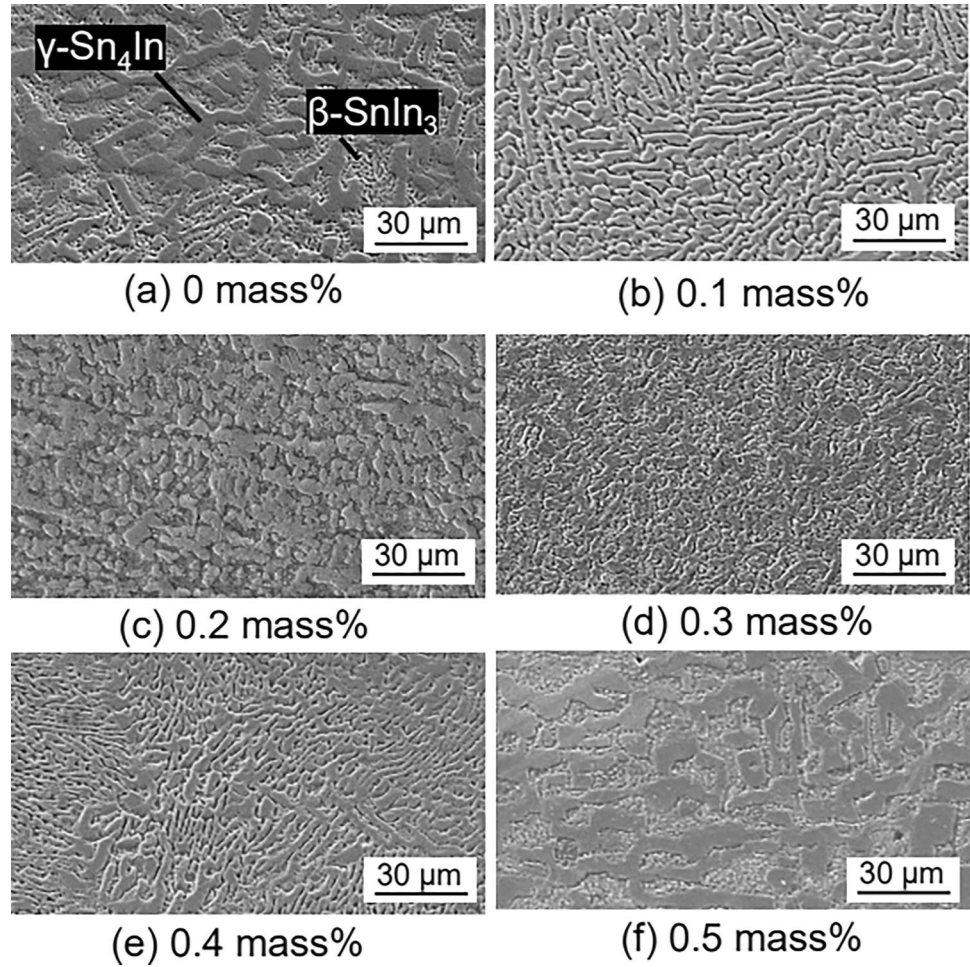
Fig. 7 Grain size measurement results of the Sn–In composite solders reinforced with 0–0.5 mass% of NiO/ZrO$_2$ nanoparticles

V-shaped angle. SEM images of the fracture surface showed that the flat area at 0 mass% was larger than that before aging. The 0.4 mass% also showed many flat areas, similar to the 0 mass% case, and no severely uneven areas were observed.

Microstructural observations were performed to investigate the effect of aging at 60 °C for 1008 h on the microstructure of Sn–In composite alloys reinforced with various ZrO$_2$/NiO nanoparticle contents. The microstructure after aging for 1008 h was observed using SEM, as shown in Fig. 10. In contrast to the initial state (Fig. 6) a coarsened and rounded γ-phase was observed in all alloys. Furthermore, the lamellar structure shown in Fig. 6 was no longer observed. Aging caused coarsening of the alloys, regardless of the addition of nanoparticles.

The average grain size of γ-phase as a function of the aging time was quantitatively evaluated, as shown in Fig. 11. The average grain size increased

Fig. 8 Tensile test results of the Sn–In composite solders reinforced with 0–0.5 mass% of NiO/ZrO$_2$ nanoparticles: **a** tensile strength and **b** elongation (Values shifted by 10 h for improved visibility)
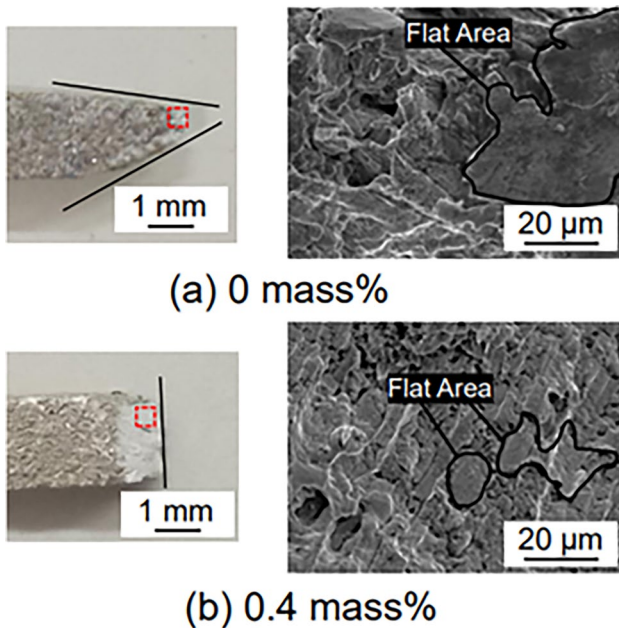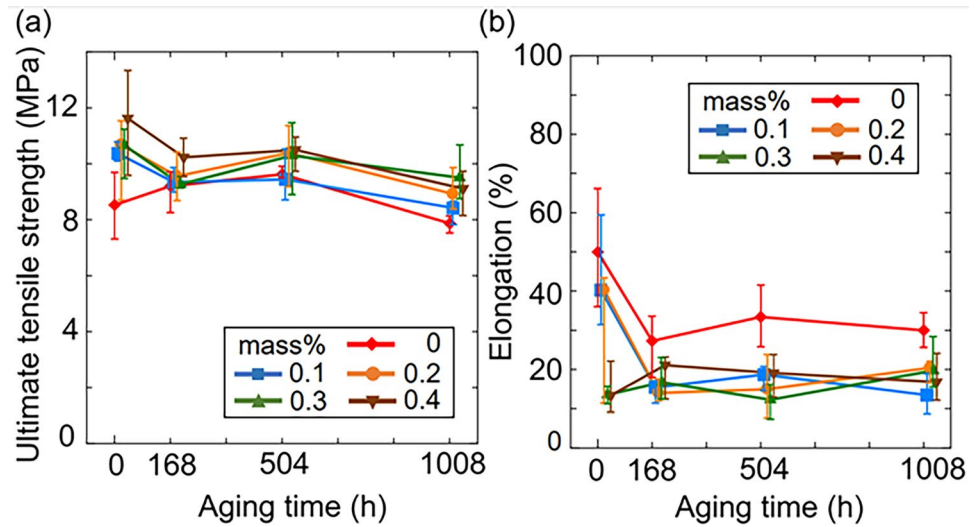
Fig. 9 Optical and SEM images of fracture surfaces of the Sn–In composite solders reinforced with **a** 0 and **b** 0.4 mass% of NiO/ZrO$_2$ nanoparticles after 1008 h aging at 60 °C

after aging for all the alloys. At 0 mass%, the average grain size increased from 15.2 μm to 17.4 μm after 1008 h. At 0.4 mass%, the average grain size increased from 4.72 μm to 16.9 μm. Furthermore, the average grain sizes of the 0 and 0.4 mass% samples after aging were similar. Based on these results, it was determined that the effect of the nanoparticle

addition on the refinement of the microstructure was limited after aging for 1008 h.

4 Discussion

4.1 Effect of nanoparticle addition on microstructure and mechanical properties

The addition of ZrO$_2$/NiO nanoparticles to a Sn–In eutectic alloy improved its mechanical properties while maintaining its melting temperature. In particular, it was found that the addition of 0.4% nanoparticles increased ultimate tensile strength by up to 35.6%. The microstructure was also refined by the addition of nanoparticles. In contrast, the elongation decreased. In this section, the mechanism of microstructural refinement by nanoparticle addition and the accompanying changes in the mechanical properties are discussed.

The Sn–In composite alloys reinforced with ZrO$_2$/NiO nanoparticles exhibit refined grains, as shown in Fig. 7. It has been widely reported that the addition of ceramic nanoparticles can refine the microstructures of various metal matrices. Wu et al. [27] demonstrated that doping with Al$_2$O$_3$ nanoparticles resulted in a finer Sn–0.3Ag–0.7Cu alloy matrix microstructure and a decrease in the thickness of the interfacial IMC layer. Rajendran et al. [28] that the addition of 0.2 mass% ZnO nanoparticles to the Sn–Bi eutectic alloy changed the coarse lamellar structure to a fine

Fig. 10 SEM microstructure images of the Sn–In composite solders reinforced with **a** 0, **b** 0.1, **c** 0.2, **d** 0.3, **e** 0.4 and **f** 0.5 mass% of NiO/ZrO$_2$ nanoparticles after 1008 h aging at 60 °C
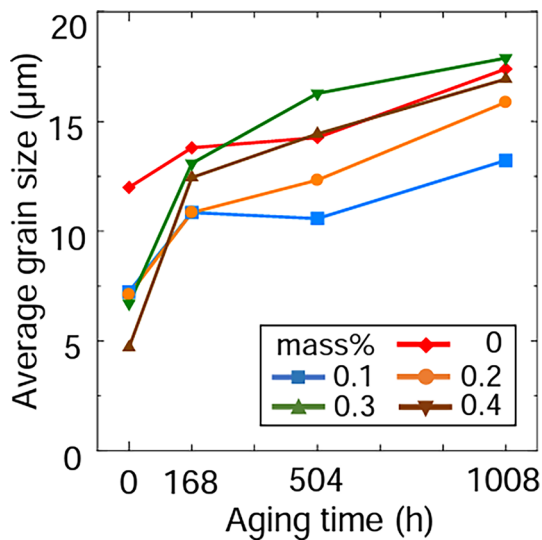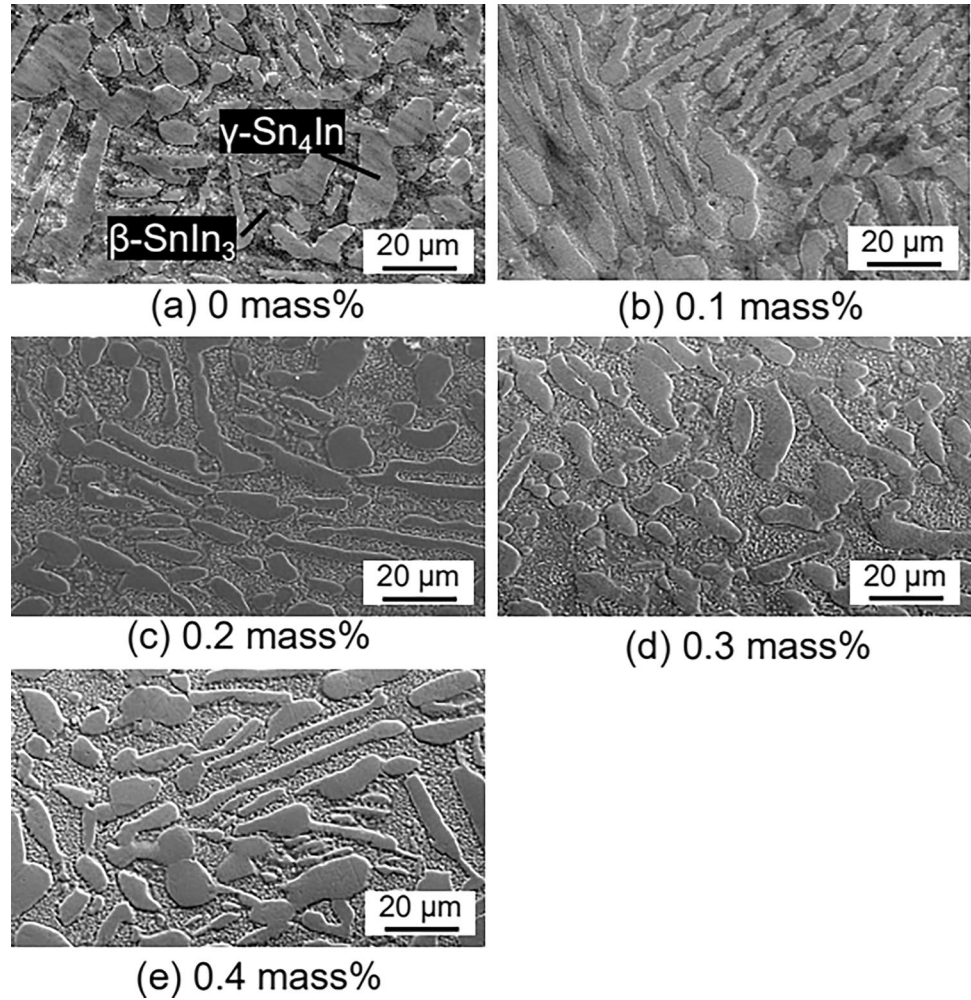
Fig. 11 Grain size evolution of γ-phase in the Sn–In composite solders reinforced with NiO/ZrO$_2$ nanoparticles during thermal aging at 60 °C

lamellar structure, and the average eutectic Fig spacing between the Sn-rich and Bi phases decreased significantly. It is believed that the nanoparticles provide nucleation sites during solidification and promote the formation of heterogeneous nuclei [29, 30]. In addition, Wu et al. reported that when tiny particles are inclined to form at the grain interface of β-Sn dendrites, they have a pinning effect on the grain boundary movement, which explains the refinement mechanism of adding nanoparticles. Moreover, excessive additions may induce agglomeration, resulting in limited refinement. This is supported by Li et al. [31], who showed that nanoparticles are highly surfactant and aggregate easily. Based on this understanding, the grain refinement behavior of the ZrO$_2$/NiO nanoparticles added in this study should be monitored at appropriate amounts.

The ZrO$_2$/NiO nanoparticles addition enhanced the ultimate tensile strength of the composite alloy for two

main reasons. The first is grain refinement strengthening, which is known as the Hall–Petch law [32]. It has been reported that yield strength and tensile strength are inversely proportional to the square root of grain size as in the following equation [Ref.].

$$\sigma = \sigma_0 + Kd^{-\frac{1}{2}}$$

where σ_0 and K are material constants. Figure 12 presents the linear regression analysis of the experimental data, the dependence of $\sigma_{0.2}$ on the reciprocal square root of d_m for the Sn–In composite solders reinforced with NiO/ZrO$_2$ nanoparticles (x = 0–0.4 mass%). Figure 12 shows that the ultimate tensile strength tends to be inversely proportional to the square root of the grain size. This suggests that the decrease in grain size is one of the reasons for the increase in strength of the Sn-In eutectic alloy.

The second is dispersion strengthening by the nanoparticles [33]. Amares et al. [20] that the strength of a Sn–Bi eutectic solder increased with the addition of ZrO$_2$ nanoparticles. They pointed out that the reason for this was the effect of alloy matrix refinement and the strengthening of the ZrO$_2$-nanoparticle dispersion. Xing et al. [15] also reported that an increase in the pinning effect and dislocation density due to the addition of nanoparticles to the linear motion of dislocations increased the strength of the alloys. Therefore, it can be concluded that the increase in the ultimate tensile strength owing to the addition of nanoparticles in this study was due to grain refinement and dispersion strengthening.
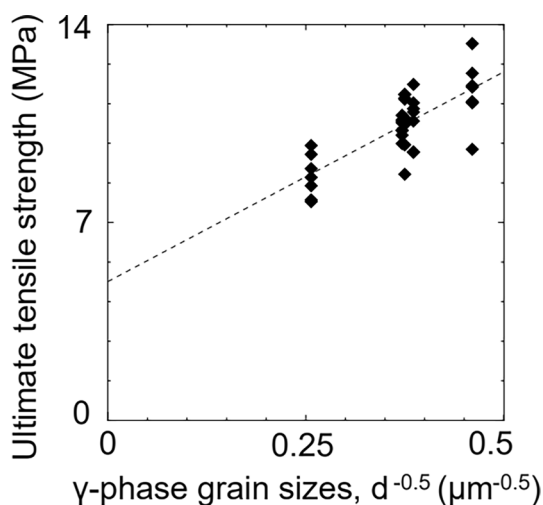
The addition of nanoparticles decreased the elongation, as shown in Fig. 4. Tsao et al. [32] reported that the addition of TiO$_2$ to Sn–0.7Cu solder reduced the elongation. This can be explained by the high microporosity along the grain boundaries and crack-generation sites in the form of hard and brittle TiO$_2$ nanopowders. Other studies by Tsao et al. [30] confirmed that the addition of TiO$_2$ nanoparticles to Sn–3.5Ag–0.25Cu solder causes microporous grain boundaries and reduced elongation owing to the presence of nano-TiO$_2$ and Ag$_3$Sn, which are second-phase particles. These findings indicate that the nanoparticles in this study may have been the initiation sites for cracks, resulting in reduced elongation.

The change in the fracture surface may be related to the γ-phase and β-phase, which are representative phases of the microstructure of Sn–In eutectic solder. γ-phase is harder than β-phase [34], which causes a difference in the elongation during tensile tests. This difference may cause only the well elongated β-phase to be visible on the fracture surface layer, whereas the less elongated γ-phase appears as a hole. Elemental analysis showed that the flat area contained the β-phase, which supports our theory. The addition of nanoparticles also reduced the spacing between adjacent γ-phases owing to the refinement of crystal grains, resulting in the appearance of severe irregularities. Figure 7 shows that the addition of 0.5 mass% of nanoparticles resulted in the same grain size as that of 0 mass%, which is presumed to be the reason for the appearance of flat areas in some parts.

4.2 Effect of thermal aging on microstructure and mechanical properties

The presence of ZrO$_2$/NiO nanoparticles in the Sn–In composite alloys resulted in superior high-temperature mechanical stability compared to that of the Sn–In eutectic alloy. After thermal aging at 60 °C, the nanoparticle reinforcements provided up to 1.2 times higher strength than that of the alloy without nanoparticle addition. However, the ZrO$_2$/NiO nanoparticle addition still resulted in a decrease in the elongation, particularly at contents of 0.3 mass% or higher. This section discusses the effects of thermal aging on the degradation of the mechanical properties of the composite alloys.

One possible degradation mechanism could be the coarsening of the γ-phase, which was found after thermal aging at 60 °C regardless of nanoparticle addition.

Fig. 12 The relationship between ultimate tensile strength of γ–phase grain sizes of the Sn–In composite

The diffusion rate can be determined based on the homologous temperature (T_h), which is the aging temperature (T_a) divided by the melting temperature (T_m). In this study, the T_h values of In and Sn are 0.78 and 0.66, respectively [35]. At this aging temperature, Han et al. [36] suggested that In and Sn atoms in the Sn–In eutectic alloy readily diffuse through β and γ grain boundaries during isothermal aging, leading to phase coarsening. A similar coarsening phenomenon occurred in Sn–In composite alloys. In the as-alloyed state, as shown in the previous section, it was presumed that the strength-enhancement mechanism by the ZrO_2/NiO nanoparticle addition was dominated by both refinement and nanoparticle-dispersion strengthening. After aging, despite its coarse microstructure, the Sn–In composite alloy reinforced with ZrO_2/NiO nanoparticles maintained an 1.11 times higher ultimate tensile strength than that of the Sn–In eutectic alloy that was not reinforced or aged at high temperatures. Therefore, the high strength retention observed in the reinforced alloys after aging at high temperatures is thought to be due to dispersion strengthening.

The coarsening after thermal aging could also affect the decrease in elongation, in particular, at 0.2 mass% or higher compositions. Lai et al. [37] that the microstructure of Sn–35Bi alloys consists of primary and eutectic phases and that crack propagation preferentially occurs in the eutectic phase, which is the soft phase. In the Sn–25Bi alloy, crack propagation was delayed because of the larger extent of the primary phase. Therefore, the size of the soft phase is critical for the fracture behavior. Within the eutectic Sn–In alloy, which consists of two phases, the soft β-phase and hard γ-phase, the morphology of the soft β-phase, which is the main crack propagation path, is critical. A schematic of the microstructural morphology during thermal aging is shown in Fig. 13. As the hard γ-phase coarsened during aging (Fig. 11), the soft β-phase also coarsened. Furthermore, the flattening of microscopic fracture surfaces due to aging may also be related to the β-phase coarsening, regardless of the addition

of nanoparticles. Therefore, it is suggested that the coarsened β-phase facilitates crack propagation. This could be one of the reasons for the decrease in elongation after aging. In addition, as mentioned in Sect. 4.1, the excessive addition of nanoparticles may cause crack initiation. This could be another reason for the decrease in elongation.

5 Conclusion

This study investigated the effects of adding NiO/ZrO_2 nanoparticles to eutectic Sn–In alloys on their microstructure and mechanical properties before and after thermal aging. The fabricated Sn–In composite alloys reinforced with NiO/ZrO_2 nanoparticles showed a melting behavior equivalent to that of the Sn–In eutectic alloy. The addition of NiO/ZrO_2 nanoparticles at 0.1–0.4 mass% provided a refined microstructure composed of γ-Sn and β-In phases. The Sn–In composite alloy reinforced with 0.4-mass%-ZrO_2/NiO nanoparticles showed a superior initial ultimate tensile strength to that of the monolithic eutectic Sn–In alloy. We believe that the strength enhancement observed in the as-alloyed state must be attributed to microstructural refinement and nanoparticle-dispersion strengthening effects. It was suggested that improving the dispersion of nanoparticles is important for achieving moderate elongation. After thermal aging at 60 °C for 1008 h, the ultimate tensile strength of the Sn–In composite alloy reinforced with 0.3-mass%-ZrO_2/NiO nanoparticles was 20.8% higher than that of the Sn–In eutectic alloy, accompanied by an elongation decrease and.

microstructure coarsening. Thus, the nanoparticle-dispersion strengthening effect could be beneficial for thermal aging reliability.

The results presented above demonstrate that the addition of NiO/ZrO_2 nanoparticles to Sn–In alloys can enhance their strength while retaining their low melting temperatures, exhibiting potential to play a significant role in various electronic packaging applications.

Fig. 13 Schematic of coarsening of microstructure in Sn–In solder during thermal aging

Author contributions

All authors contributed to the study conception and design. Material preparation, data collection and analysis were performed by Shunya Nitta. The first draft of the manuscript was written by Shunya Nitta and all authors commented on previous versions of the manuscript. All authors read and approved the final manuscript.

Data availability

The datasets generated during and/or analyzed during the current study are available from the corresponding author on reasonable request.

Declarations

References

1. X. Li, H. Andersson, J. Sidén, T. Schön, Flex. Print. Electron. **3**, 015003 (2018)
2. T. Aizawa, K. Okagawa, M. Kashani, J. Mater. Process. Technol. **213**, 1095 (2013)
3. M. Layani, S. Magdassi, J. Mater. Chem. **21**, 15378 (2011)
4. V. Zardetto, T.M. Brown, A. Reale, A. Di Carlo, J. Polym. Sci., Part B: Polym. Phys. **49**, 638 (2011)
5. L. Sun, L. Zhang, Adv. Mater. Sci. Eng. **2015**, e639028 (2015)
6. Y. Zhang, Z. Cai, J. C. Suhling, P. Lall, and M. J. Bozack, in *2008 58th Electronic Components and Technology Conference* (2008), pp. 99–112.
7. JIS Z 3282 (2017)
8. B.-S. Yim, J.I. Lee, Y. Heo, J. Kim, S.H. Lee, Y.-E. Shin, J.-M. Kim, Mater. Trans. **53**, 2104 (2012)
9. H. Kang, S.H. Rajendran, J.P. Jung, Metals **11**, 364 (2021)
10. Y. Liu, K.N. Tu, Mater. Today Adv. **8**, 100115 (2020)
11. D. Le Han, Y.-A. Shen, S. Jin, H. Nishikawa, J. Mater. Sci. **55**, 10824 (2020)
12. F. Huo, Z. Jin, D. Le Han, K. Zhang, H. Nishikawa, Mater. Des. **210**, 110038 (2021)
13. S. Cai, X. Luo, J. Peng, Z. Yu, H. Zhou, N. Liu, X. Wang, Adv. Compos. Hybrid Mater. **4**, 379 (2021)
14. K. Kanlayasiri, M. Mongkolwongrojn, T. Ariga, J. Alloys Compd. **485**, 225 (2009)
15. W. Xing, X. Yu, H. Li, L. Ma, W. Zuo, P. Dong, W. Wang, M. Ding, J. Alloy. Compd. **695**, 574 (2017)
16. L. Yang, S. Quan, C. Liu, H. Xiong, J. Nanosci. Nanotechnol. **20**, 2573 (2020)
17. S.H. Rajendran, S.J. Hwang, J.P. Jung, Metals **10**, 1295 (2020)
18. J. Shen, Y.C. Liu, Y.J. Han, Y.M. Tian, H.X. Gao, J. Electron. Mater. **35**, 1672 (2006)
19. T. Takemoto, J. Japan Weld. Soc. **75**, 583 (2006)
20. S. Amares, R. Durairaj, and S. H. Kuan, Arch. Metall. Mater. 407 (2021).
21. F. Huo, Y.-A. Shen, S. He, K. Zhang, H. Nishikawa, Vacuum **191**, 110370 (2021)
22. Y. Hirata, C. Yang, S. Lin, H. Nishikawa, Mater. Sci. Eng., A **813**, 141131 (2021)
23. S.Y. Chang, C.C. Jain, T.H. Chuang, L.P. Feng, L.C. Tsao, Mater. Des. **32**, 4720 (2011)
24. C.D. Beachem, G.R. Yoder, Metall. Mater. Trans. B **4**, 1145 (1973)
25. P.J. Noell, J.D. Carroll, B.L. Boyce, Acta Mater. **161**, 83 (2018)
26. J.W. Morris, J.L.F. Goldstein, Z. Mei, JOM **45**, 25 (1993)

27. J. Wu, S. Xue, J. Wang, M. Wu, J. Alloys Compd. **784**, 471 (2019)

28. S.H. Rajendran, H. Kang, J.P. Jung, J. Mater. Eng. Perform. **30**, 3167 (2021)

29. J. Wu, S. Xue, J. Wang, J. Wang, S. Liu, J. Mater. Sci. Mater. Electron. **28**, 10230 (2017)

30. L.C. Tsao, S.Y. Chang, Mater. Des. **31**, 990 (2010)

31. Y. Li, Z. Deng, Acc. Chem. Res. **52**, 3442 (2019)

32. L.C. Tsao, C.H. Huang, C.H. Chung, R.S. Chen, Mater. Sci. Eng. A **545**, 194 (2012)

33. J. Shen, Y.C. Chan, Microelectron. Reliab. **49**, 223 (2009)

34. V. Shepelevich and J. Wang, Inorg. Mater. **48**, (2012).

35. J. Evans, *A Guide to Lead-Free Solder: Physical Metallurgy and Reliability* (Springer, 2007).

36. D. L. Han, H. Tatsumi, F. Huo, and H. Nishikawa, in *2022 IEEE 72nd Electronic Components and Technology Conference (ECTC)* (2022), pp. 2148–2152.

37. Z. Lai, D. Ye, J. Mater. Sci. Mater. Electron. **27**, 3182 (2016)